MINAR International Journal of Applied Sciences and Technology
ISSN: 2717-8234
Article type: Article Review

Received: 22/09/2023 **Accepted:** 25/10/2023 **Published:** 01/12/2023

NUCLEAR STRUCTURE STUDY OF THE HALO NUCLEI

Ahmed N. ABDULLAH[1]
University of Baghdad – Iraq

Abstract

The existence of halo nuclei is one of the major important discoveries in the field of nuclear physics. These nuclei are treated as loosely bound system in which a core of normal nuclear density is surrounded by so-called neutron (or proton) halo of diluted nuclear matter. Many theoretical investigations have attempted to understand these nuclei, which exist at light to heavy masses. The phenomenon of nuclear halo is a quantum effect that occurs in nuclei due to the presence of valence nucleons with low separation energy and I = 0, 1 (low angular momentum), and is manifested by the extraordinarily large radii of these nuclei. The core plus halo model is commonly used to describe halo nuclei. This model recognizes the need to treat the core and the halo neutrons or protons separately. By considering different model spaces for the core and the halo nucleons, we can better explain the properties of halo nuclei. This separation is justified by the fact that the valence nucleons in a halo nucleus have different properties compared to the core. Halo nuclei at rest cannot be used as target due to their short-lived species and extraordinary ratio of neutrons and protons (either neutron-rich or proton-rich). Instead, they can be studied through direct reactions with a radioactive isotope beam, employing inverse kinematics where the role of the beam and target are exchanged. In order to investigate the charge and matter densities of these nuclei, total and differential reaction cross section analyses of proton scattering on halo nuclei have been carried out using various theoretical and phenomenological methods**.**

Keywords: *Halo Nuclei, Root Mean Square Radii, Exotic Nuclei, Density Distributions*.

http://dx.doi.org/10.47832/2717-8234.17.18

[1] ahmed.n@sc.uobaghdad.edu.iq

1.Introduction

For many years, the scattering of hadrons and leptons from nuclei has provided valuable information about the matter and charge distributions of stable nuclei near and on the line of stability. The development of radioisotope beam method has opened up new fields to study unstable nuclei far away from the line of stability [1-3]. This extends our knowledge for nuclear physics from stable to unstable nuclei. Experiments with radioisotope beams have been show that the features of unstable nuclei are significantly different from those of stable nuclei [4]. Therefore, it is very interesting to study theoretically the features of unstable nuclei using reliable theories and models. The research results will provide a reference for future experiments and reliability testing of the established unstable nuclear theory [5].

2. Drip Line Nuclei

The number of neutrons and protons in the nucleus are used to study the matter properties. Specifically, the protons number (Z) identifies the various elements, ranging from hydrogen to uranium. Each element can exist in nature as a variety of isotopes depending on the neutrons number (N). There are 92 stable elements found in nature, along with nearly 300 stable isotopes. When represented in the chart of nuclides (Fig. 1), where the protons number (Z) is plotted against the neutrons number (N), the stable nuclei tend to align along the diagonal from the lower left to the upper right, known as the valley of stability. This diagram is also referred to as the nuclear landscape [6].

We can be classified the nuclear landscape into three main areas. The first area, indicated by black dots, represents stable nuclei with an infinite lifetime. These stable nuclei are typically found around the line of stability, where N≈Z. The second area is the proton drip line, situated above the line of stability as shown in Fig. 1. Nuclei along this line are known to be proton-rich. The final area is the neutron drip line, located at the lower end of the line of stability. Nuclei along this line are known to be neutron-rich. Scientists in this field refer to the region beyond the proton-rich and neutron-rich areas as the edge of stability, where nuclei become unbound [7-9].

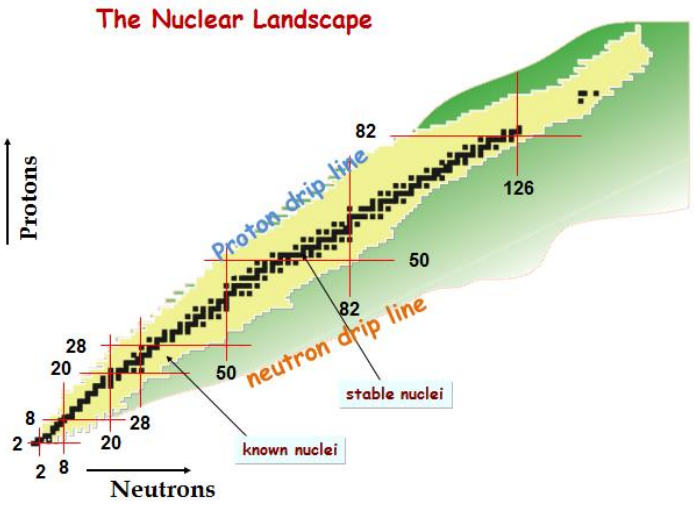

Fig. 1: The chart of nuclides [6].

Unstable nuclei lie far from the line of stability, in the region of the proton and neutron drip lines, which are defined as the limits beyond which nuclei become unstable. Nuclei close to the drip lines are often called exotic nuclei because of their distance from the stability valley, denoting entities that differ from the most ordinary nuclei found in nature [8].

3. Exotic nuclei

In modern nuclear physics, the study of exotic nuclei is one of the most exciting research areas due to the decay modes and structure of many nuclei far from the line stability are remain unknown. At many research facilities around the world, the nuclear properties of these radioactive nuclei are of great interest to experimentalists. The properties and nuclear structures of nuclei along the neutron or proton drip lines can be highly unusual and therefore challenge our conventional knowledge gained from experiences with nuclei near or at stability [10].

Exotic nuclei are the nuclei with an unusual nucleonic composition. A characteristic feature of exotic nuclei is that they lie far from the valley of stability and have an abnormal N/Z ratio, meaning that they have an excess of neutrons or protons compared to stable nuclei; thus, these nuclei are called neutron-rich nuclei or proton-rich nuclei [11, 12].

The ratio of N/Z in stable nuclei is limited to 1-1.5 and the separation energy of a nucleon, either a neutron or a proton is almost always 6-8 MeV. Due to these boundaries and the stability, neutrons and protons in stable nuclei mix homogeneously and no decoupling of neutron and proton distributions was observed. On the contrary, the N/Z in unstable nuclei can vary from 0.6 to 4 and the separation energy can be varied from 40 MeV to 0. These variations lead to the decoupling of neutron and proton distributions as halo and skin [13].

Figs. 2 (a) and (b) show the potential difference between the stable and unstable neutron rich nuclei, respectively. In each figure, the proton potential is shown on the left side for y-axis and the neutron potential is shown on the right. The proton and neutron potentials in stable nuclei are the same except that the proton potential is shallower due to Coulomb interaction. The separation energy of neutrons and protons is almost the same. The potential of protons becomes deeper when the excess neutrons number increases due to the attractive p-n interactions. Therefore, the proton separation energy becomes large. On the contrary, the neutron separation energy becomes smaller and is close to zero at the neutron drip line. The neutron density shows a long tail, known as a neutron halo, that extends many times further than the normal density tail when the neutron separation energy is less than 1 MeV. Although the proton halo forms in some proton drip line nuclei, it is not pronounced as neutron halo [13].

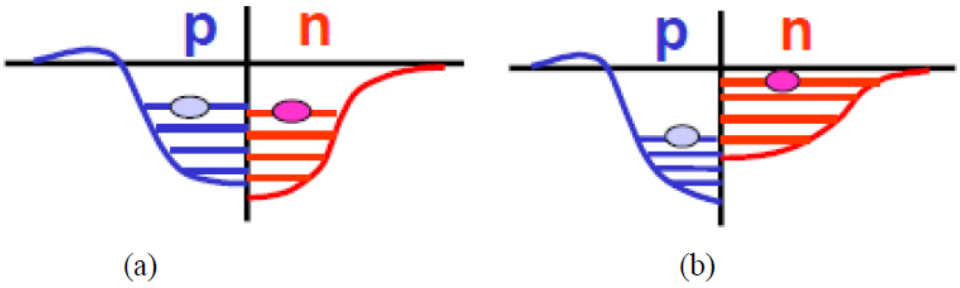

Fig. 2: The potential difference between the (a) stable nucleus (b) unstable neutron rich nucleus [6].

Study on the structure of exotic nuclei is of particular interest for possible existence of skin and halo nuclei. Meanwhile, the study of exotic nuclear structure extends from proton-rich region to neutron-rich region [14]. Skin and Halo nuclei have their anomalous structures that stable nuclei do not have. The former is the layer of nucleons on the nuclear surface, while the latter is the expanded density of valence nucleon(s) outside of the core nucleus. These structures are exotic features because in a stable nucleus neutrons and protons are uniformly mixed [15].

4. Skin and halo nuclei

Tanihata *et al.* [15] reported that an unexpected exotic type of nuclei reveals by the structure of nuclei at the neutron-dripline. This type of nuclei was discovered in 1985 at Lawrence Berkeley National Laboratory. Experiments provide evidence that that the lithium isotope ^{11}Li, which is the most unstable and neutron-rich, has an unusually large size is comparable to a heavy nucleus like lead, with 208 nucleons (Fig. 3). These observations have been challenging the naive belief that the nucleus radius depends on the mass number only (nucleons total number) in a compact structure, where all the neutrons and protons over the nuclear volume are distributing uniformly. It was found that the two extra loosely-bound

neutrons in this lithium isotope in a diluted and extended distribution around the core nucleus ^{9}Li forming the neutron halo, this term introduced by Hansen and Jonson [16]. In this case, the neutrons halo has a large probability to be very far away from the core, in the classical forbidden region. Therefore, the term neutron-rich halo nuclei refer to all types of nuclei which have structure similar to nucleus ^{11}Li in where one or more neutrons are located far away from the core. Many other nuclear systems with neutron halos that are lie away from the stability line are observed after the experimental discoveries of a two neutrons halo in ^{11}Li [17–19].

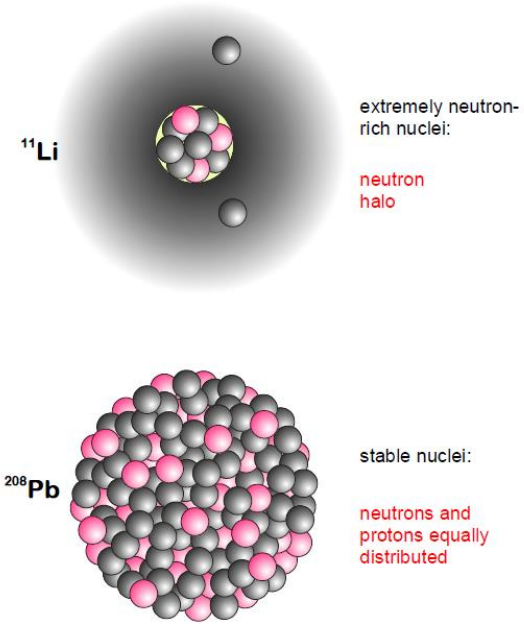

Fig. 3: The neutron halo nucleus ^{11}Li compared with the size of ^{208}Pb nucleus [20].

All these studies finally give the picture of halo nucleus. A strongly bound core surrounded by halo nucleons, either neutrons or protons. In other words, these exotic nuclei are made up of thin cloud of nucleons that orbit other nucleons form the core at large distances. The term halo is originally taken from the analogy of the halo of the moon and sun (bands of light around the moon and sun) (Fig. 4). The cause of the halo phenomenon is the low separation energy of the outer nucleons and the orbits they occupy with l = 0, 1 (low angular momentum), which allows the halo nucleons wave function to expand to large radii. The term halo originally came from the analogy of the halo (bands of light around the moon and sun) of the moon and sun. Tanihata's observations of large total interaction cross sections for ^{11}Be, ^{11}Li and ^{14}Be suggested the possible presence of halos in many other neutron-rich nuclei near the drip-line. This behavior is also evident on the side of proton-rich for the nuclear chart. But compared to neutron-rich nuclei, proton-rich nuclei are rarely studied. It is thought that it is slightly more difficult for proton-rich nuclei to form halo structures because the Coulomb barrier prevents the protons to penetrate into the outer regions of the core [21-24].

Fig. 4: The halo phenomena (left), and the halo of moon (right) [25].

Generally, the halo nucleus has a large excess of neutrons or protons, where some outer nucleons bound very weakly. These halo systems can be described by the model of few-body, which considered that the halo nucleus consists of an inner core with few loosely bound outer nucleons (protons or neutrons). Therefore, we can be divided the halo nuclei into two kinds: two-body halos, in which one nucleon surround the core, likely the ^{11}Be (one-neutron halo) and ^{8}B (one-proton halo); and three-body halos, in which the core is surrounded by two valence nucleons, likely ^{6}He and ^{11}Li (two-neutron halo) [26, 27] (Fig. 5).

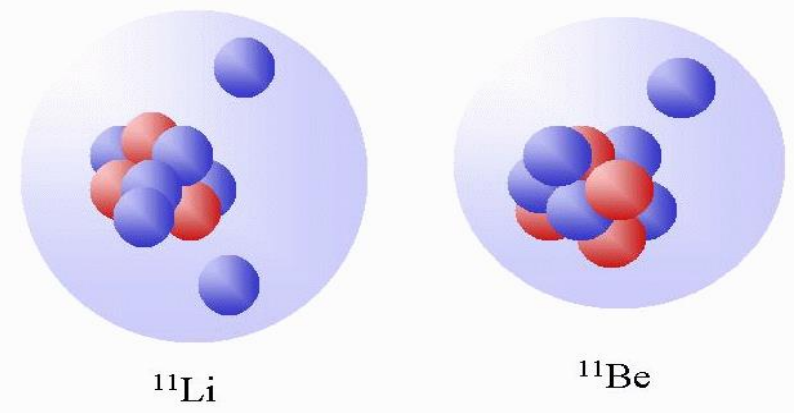

Fig. 5: The two-body halo ^{11}Be and three-body halo ^{11}Li [28].

The nuclear density three basic rules of nuclei close to the stability valley are broken in the halo nucleus [29]:

The first rule is that the radius at which the nuclear density decreases to half its maximum density is given by $R = R_0 A^{1/3}$. The second one is that neutrons and protons in the nucleus are mixed homogenously ($\rho_n \approx \rho_p$), this only applies to the core for halo nucleus. Finally, the distance over which the nuclear density decreases from 90% to 10% of the

maximum value, the so-called surface thickness, is constant, approximately $t \approx 2.3$ fm (Fig. 6). This feature applies to nuclei in the stability valley because the separation energy of nucleon (6–8 MeV) of stable nuclei is nearly constant. Generally, surface diffuseness or surface thickness is expected to depend on the separation energy of nucleon. Neutron halos are the case where small separation energies less than 1 MeV are most evident [29].

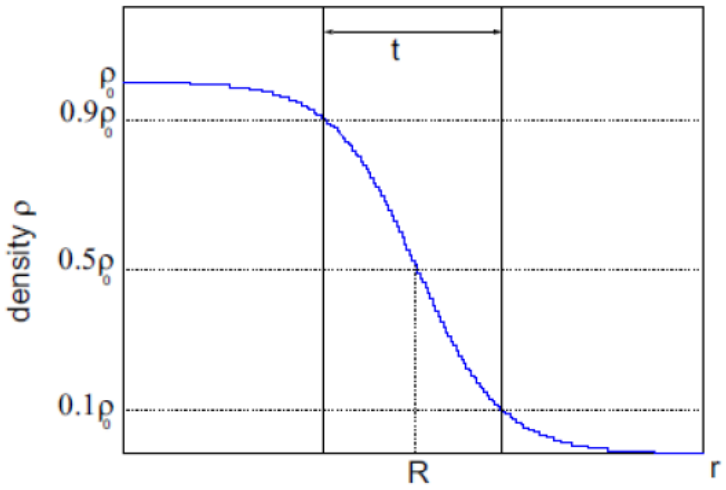

Fig. 6: Nuclear density with the definition for surface thickness t [29].

5. Density distributions and interaction cross sections

The main method used to determine the density distributions and matter radii of exotic nuclei is measurement of reaction (σ_R) and interaction (σ_I) cross sections. In fact, the σ_I measurements of isotopes He and Li are led to the first observation of the halo phenomena [15, 30, 31]. This has been possible because the Glauber model success to calculate the cross section [32].

The σ_R using Glauber model with optical limit is given as [33]:

$$\sigma_R = 2\pi \int_0^\infty b\, db\, [1 - T(b)] \qquad (1)$$

where $T(b)$ is the transparency function given as:

$$T(b) = exp\left[-\sum_{ij} \sigma_{ij} \int \rho_{Ti}^z(s)\rho_{Pj}^z(|b-s|)ds\right] \qquad (2)$$

$$\rho_{Ti}^z(s) = \int_{-\infty}^{\infty} \rho_{ki}\left(\sqrt{s^2+z^2}\right) dz \qquad (3)$$

The index $k = \mathrm{T}$ (target) or P (projectile) and σ_{ij} is the total cross section of nucleon–nucleon in which indices i, j are refer to neutron and proton.

For nucleus-nucleus collisions, although this is one of the most basic forms of the Glauber model, but it is still capable of reproducing the fragmentation and reaction cross sections over a wide energy range as noticed in Fig. 7. This method is tested in an energy

range from 30A to 800A MeV with incident ^{12}C on targets ^{9}Be, ^{12}C and ^{27}Al. The measured cross sections are shown in Fig. 7. In this figure the dash-dotted curves refer to the σ_R obtained by the calculations of optical limit using densities for those stable nuclei [33].

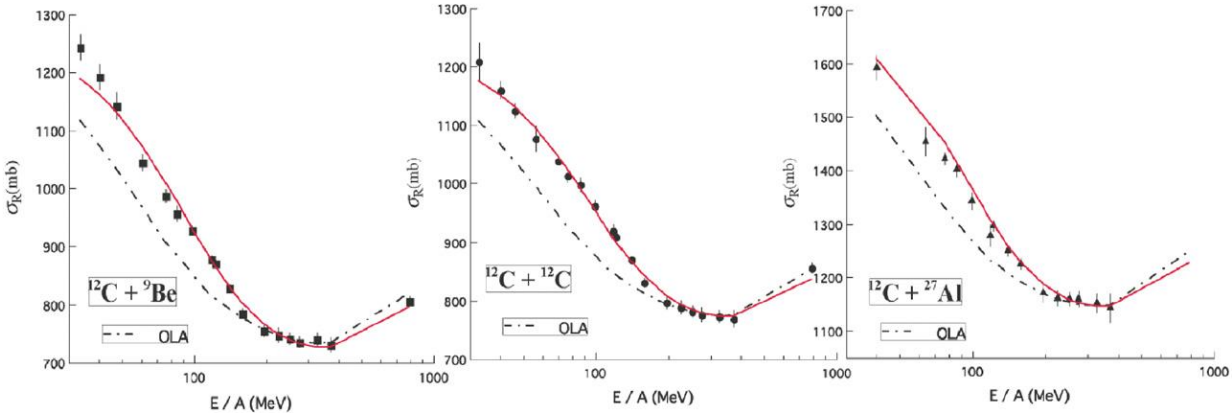

Fig. 7: Energy dependence of the σ_R [33].

6. Density distributions and elastic scattering

Elastic proton scattering with high energy is assumed the best away to obtain the density distribution of nuclear matter. Using the liquid hydrogen target system IKAR, elastic proton scattering cross section on different halo nuclei are studied at GSI. For $^{6,8}He$ and $^{8,9,11}Li$, the matter density distributions have been found. Fig. 8 displays the determined matter density distribution for ^{6}He and ^{8}He. The obtained rms matter radii for ^{6}He and ^{8}He are $(R_m = 2.45 \pm 0.10)$ and $(R_m = 2.53 \pm 0.08)$ fm, respectively which consistent with the results obtained from the σ_I. The same type of experiments was performed on Li isotopes [34-36].

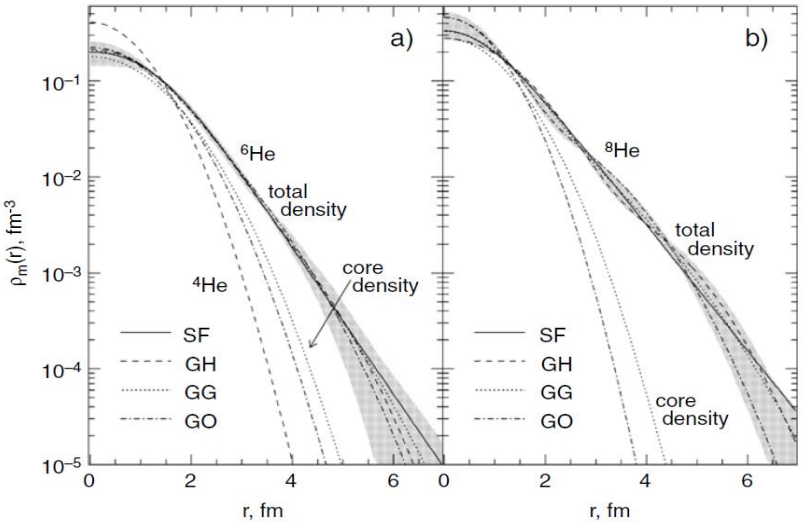

Fig. 8. Density distributions of ^{6}He and ^{8}He [36].

Fig. 9 displays the differential cross sections ($d\sigma/dt$) of Li isotopes. These cross sections are used to calculate the matter radii and density distributions. Fig. 10 compares the density distributions determined by the σ_I and proton elastic scattering. So far, these measurements are limited to light elements. Extending these measurements to include heavier nuclei will be provided interesting information into nuclear structure [33].

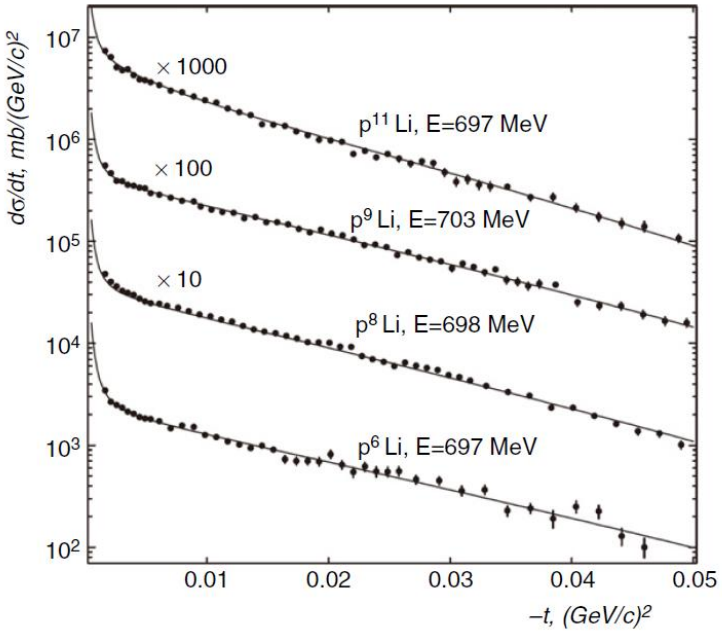

Fig. 9: $d\sigma/dt$ for Li isotopes [35].

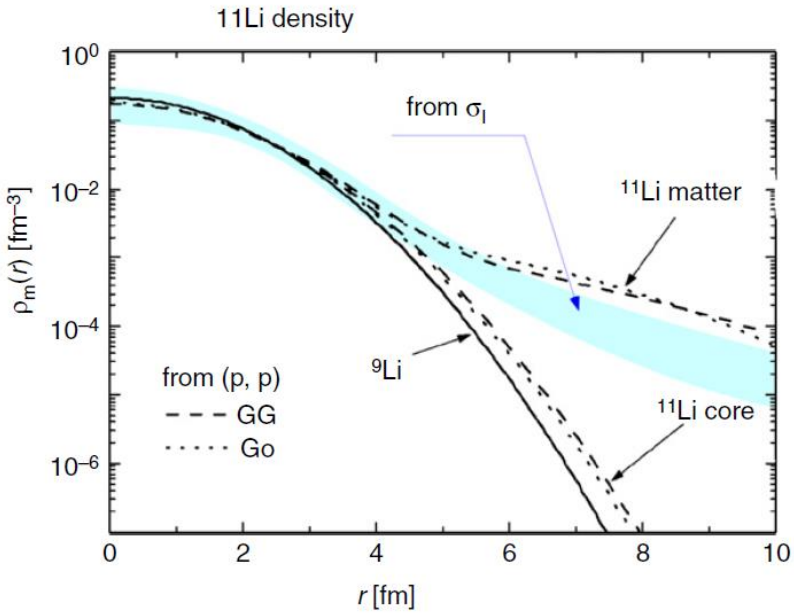

Fig. 10: Density distributions obtained by σ_I (shadowed area) and proton scattering (lines) [33].

7. The density distributions parametrizations

The following phenomenological density distributions can be used to study the elastic-scattering cross sections (proton + halo nucleus). These model density distributions, labeled as GG (Gaussian–Gaussian), SF (Symmetrized Fermi), GH (Gaussian–Halo), and GO (Gaussian–Oscillator) [36]:

1- The GG parametrization

The core and halo density distributions are given by the Gaussian function [36]:

$$\rho_j(r) = \left(\frac{3}{2\pi R_j^2}\right)^{3/2} exp\left(-\frac{3r^2}{2R_j^2}\right) \ , j = c, h \qquad (4)$$

where $R_c$and R_h are the core and halo rms radii and ρ_h, respectively. The total matter density distribution ρ_m is given by [36]:

$$\rho_m(r) = \frac{[4\rho_c(r) + (A-4)\rho_h(r)]}{A} \qquad (5)$$

and

$$R_m = \left[\frac{4R_c^2 + (A-4)R_h^2}{A}\right]^{1/2} \qquad (6)$$

2- The SF parametrization

The SF distribution of the matter density is given by [36]:

$$\rho_m(r) = \frac{3}{4\pi R_0^3}\left[1 + \left(\frac{\pi a}{R_0}\right)^2\right]^{-1} \sinh\left(\frac{R_0}{a}\right) \Big/ \left[\cosh\left(\frac{R_0}{a}\right) + \cosh\left(\frac{r}{a}\right)\right] \qquad (7)$$

Where a is the parameter of diffuseness and R_0 is half-density radius. The R_m is connected with the parameters R_0 and a by the relation:

$$R_m = \left(\frac{3}{5}\right)^{1/2} R_0\left[1 + \frac{7}{3}\left(\frac{\pi a}{R_0}\right)^2\right]^{1/2} \qquad (8)$$

3- The GH parametrization

The explicit expression for the GH density distribution is [36]:

$$\rho_m(r) = \left(\frac{3}{2\pi R_m^2}\right)^{3/2} [1 + \alpha\varphi(r)]\, exp\left(-\frac{3r^2}{2R_m^2}\right) \qquad (9)$$

With

$$\varphi(r) = \frac{3}{4}\left[5 - 10\left(\frac{r}{R_m}\right)^2 + 3\left(\frac{r}{R_m}\right)^4\right] \qquad (10)$$

4- The GO parametrization

The Gaussian and $1p$-shell HO distributions are used for the core and halo densities, respectively [36]:

$$\rho_h(r) = \frac{5}{3}\left(\frac{5}{2\pi R_h^2}\right)^{3/2} \left(\frac{r}{R_h}\right)^2 exp\left(-\frac{5r^2}{2R_h^2}\right) \qquad (11)$$

8. Charge and proton radii of halo nucleus

The measurements of isotope shift, muonic atoms and electron scattering have been used to determine Charge or proton radii of nuclei. For unstable nuclei, the rms charge radii are mostly determined by isotope shift measurements [33]. In a nucleus the point proton radius is determined from the charge radius using the equation,

$$\langle r_c^2 \rangle = \langle r_p^2 \rangle + \langle R_p^2 \rangle + \frac{N}{Z}\langle R_n^2 \rangle + \frac{3\hbar^2}{4m_p^2 c^2} \qquad (12)$$

where R_n and R_p are the free neutron and proton charge radii, respectively, $R_n^2 = -0.1161 \pm 0.0022$ fm^2 and $R_p^2 = 0.769 \pm 0.012$ [33].

Table 1 and Figs. 11–13 display the obtained results of the point nucleon radii taken from [33]. From these results we can be seen that when a neutron halo is formed the proton radius increases (^{4}He → ^{6}He, ^{9}Li → ^{11}Li, and ^{10}Be → ^{11}Be) [33].

Table 1: The calculated radii of isotopes He, Li, and Be [33].

	A	$\langle r_c^2 \rangle^{1/2}$	$\langle r_p^2 \rangle^{1/2}$	$\langle r_m^2 \rangle^{1/2}$	$\langle r_n^2 \rangle^{1/2}$	$\langle r_n^2 \rangle^{1/2} - \langle r_p^2 \rangle^{1/2}$
	4	1.676 ± 0.008	1.457 ± 0.010	1.457 ± 0.010	1.457 ± 0.010	0
He	6	2.068 ± 0.01	1.925 ± 0.012	2.50 ± 0.05	2.74 ± 0.07	0.82 ± 0.07
	8	1.929 ± 0.026	1.807 ± 0.028	2.52 ± 0.03	2.72 ± 0.04	0.91 ± 0.05
	6	2.517 ± 0.030	2.38 ± 0.03	2.36 ± 0.03	2.34 ± 0.07	-0.03 ± 0.08
	7	2.39 ± 0.03	2.25 ± 0.03	2.33 ± 0.05	2.39 ± 0.09	0.14 ± 0.09
Li	8	2.30 ± 0.03	2.16 ± 0.03	2.39 ± 0.06	2.52 ± 0.09	0.35 ± 0.10
	9	2.22 ± 0.04	2.08 ± 0.04	2.34 ± 0.06	2.46 ± 0.09	0.37 ± 0.09
	11	2.47 ± 0.04	2.37 ± 0.04	3.5 ± 0.09	3.84 ± 0.11	1.48 ± 0.12
	7	2.647 ± 0.017	2.548 ± 0.018	2.31 ± 0.02	2.21 ± 0.03	-0.34 ± 0.04
	9	2.519 ± 0.012	2.403 ± 0.012	2.38 ± 0.01	2.368 ± 0.016	-0.03 ± 0.02
Be	10	2.357 ± 0.018	2.284 ± 0.019	2.30 ± 0.02	2.304 ± 0.025	0.02 ± 0.03
	11	2.463 ± 0.016	2.361 ± 0.017	2.91 ± 0.05	3.09 ± 0.06	0.73 ± 0.07
	12			2.59 ± 0.06		
	14			3.10 ± 0.15		

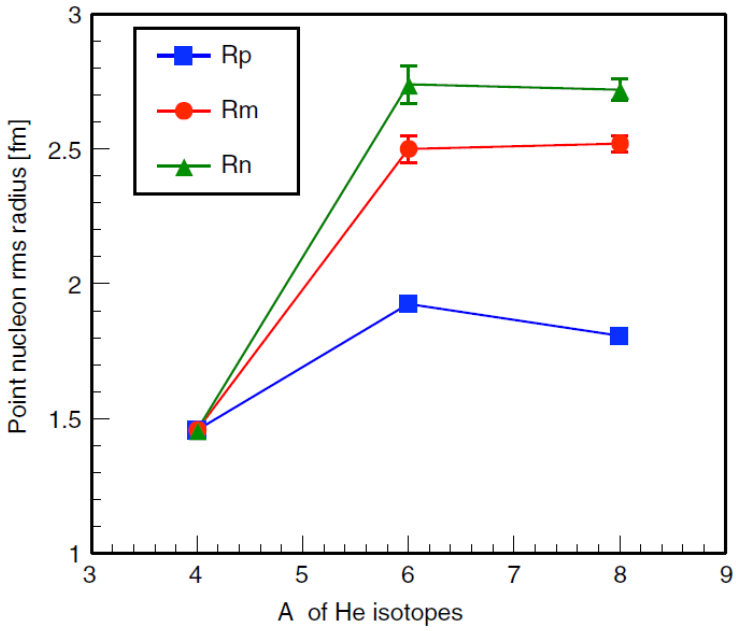

Fig. 11: Nucleon (R_m), proton (R_p) and neutron (R_n) rms radii of He isotopes [33].

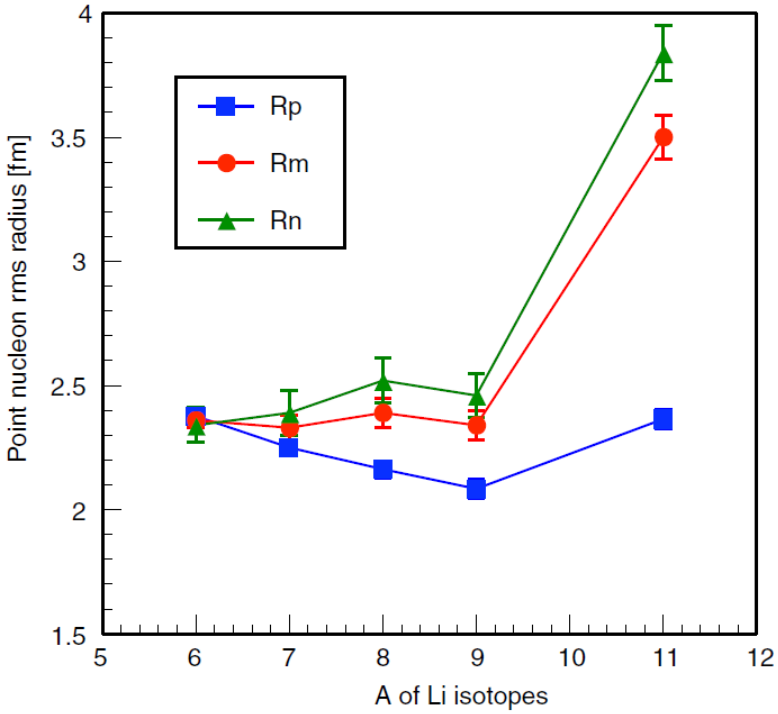

Fig. 12: Same as Fig. 11 for Li isotopes [33].

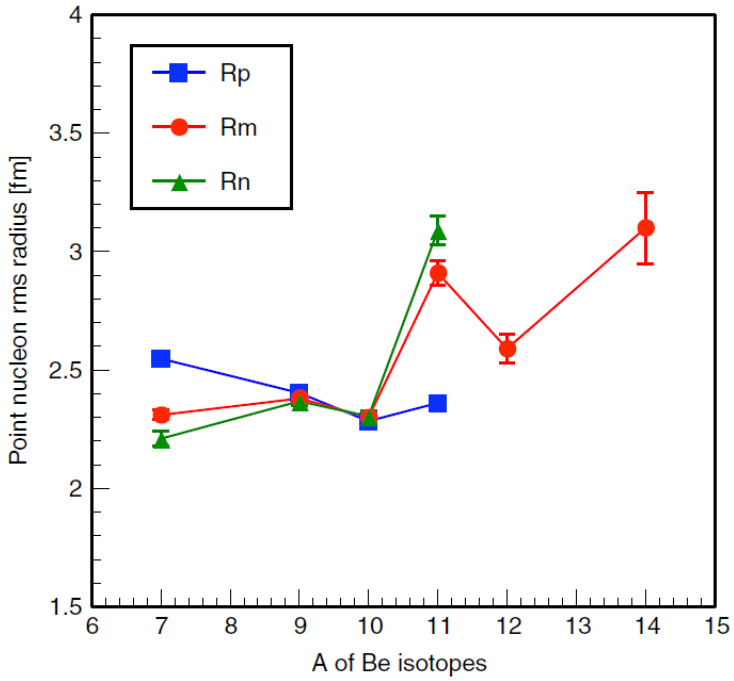

Fig. 13: Same as Fig. 11 for Be isotopes [33].

9. Articles on halo nuclei

Table 2 displays the previous articles studied the ground state properties such as the proton $[\rho_p(r)]$, neutron $[\rho_n(r)]$ and matter $[\rho_m(r)]$ density distributions and the corresponding rms radii of halo nuclei using different models, such as the Glauber model (GM), Two-Frequency Shell Model (TFSM), Binary Cluster Model (BCM), Three-Body Model of Core + $2n$

(TBMCNN), Two-Body Model of Core + n (TBMCN) and Two-Body Model of Core +p (TBMCP). The long tail manner was clearly seen in the calculated $\rho_n(r)$ and $\rho_m(r)$ for neutron-rich halo nuclei. While the long tail manner is clearly seen in the calculated $\rho_p(r)$ and $\rho_m(r)$ for proton-rich halo nuclei. The results obtained provide the halo structure of nuclei under study.

Table 2: previous studies

Ref.	Author name	Model used	Nuclei under study	Type of Nuclei
[37]	Tanaka *et al.* (2010)	GM	^{17}Ne	Two – proton halo
[38]	Hamoudi *et al.* (2014)	BCM and TFSM	^{8}He and ^{17}B	Two – neutron halo
[39]	Hamoudi and Abdullah (2016)	BCM	^{11}Li and ^{12}Be	Two – neutron halo
[40]	Du *et al.* (2016)	GM	^{15}C and ^{16}C	One – and two – neutron halo, respectively
[41]	Abdullah (2017)	TBMCNN with Woods-Saxon (WS) wave functions	^{6}He, ^{11}Li, ^{12}Be and ^{14}Be	Two – neutron halo
[42]	Korolev *et al.* (2018)	GM	^{8}B	One – proton halo
[43]	Abdullah (2018)	BCM and TFSM	^{6}He and ^{11}Li	Two – neutron halo
[44]	Abdullah (2020)	TBMCN with cosh potential wave functions	^{14}B, ^{15}C, ^{19}C and ^{22}N	One – neutron halo
[45]	Abdullah (2020)	TBMCNN with Bear–Hodgson (BH) potential wave functions	^{6}He, ^{11}Li, ^{14}Be and ^{17}B	Two – neutron halo
[46]	Abdullah (2020)	TBMCNN with cosh potential wave functions	^{6}He, ^{11}Li, ^{14}Be and ^{17}B	Two – neutron halo
[47]	Sultan and Abdullah (2021)	BCM	^{23}Al and ^{27}P	One – proton halo
[48]	Sallh and Abdullah (2021)	TBMCNN with the HO and WS wave functions	^{8}He and ^{26}F	Two – neutron halo
[49]	Mahdi and Abdullah (2022)	TBMCN with WS and GS wave functions	^{18}N and ^{20}F	One – neutron halo
[50]	Abdullah (2022)	TBMCP with BH potential wave functions	^{8}B, ^{12}N, ^{23}Al and ^{27}P	One – proton halo
[51]	Mahdi and Abdullah (2023)	TBMCN within WS and GS wave functions	^{8}Li and ^{11}Be	One – neutron halo
[52]	Mahdi and Abdullah (2023)	TBMCP within WS and GS wave functions	^{9}C and ^{12}N	One – proton halo

10. Summary and Conclusions

We have attempted to include as many experimental and theoretical investigations of halo nuclei as we possibly also providing an explanation of the physics behind the scenes. An overview of the studies is provided below:

1. It has been observed that several nuclei have (i) one- neutron halo such as ^{14}B, ^{15}C, ^{19}C and ^{22}N (ii) two- neutron halo such as ^{6}He, ^{11}Li, ^{14}Be and ^{17}B (iii) one- proton halo such as ^{8}B, ^{12}N, ^{23}Al and ^{27}P (iv) two- proton halo such as ^{17}Ne.

2. It is thought that both a small binding energy and l = 0, 1 (low angular momentum) for the outer nucleons led to the neutron halo in nuclei.

3- In halo nuclei, a decoupling of the neutron and proton distributions is strongly suggested.

4-These different models (referred to in this article) provide a good description of the nuclear structure for halo nuclei according to the calculated results.

5- The typical property of halo structure is the long tail performance.

6- For neutron-rich halo nuclei, the long tail manner was clearly seen in the calculated $\rho_n(r)$ and $\rho_m(r)$.

7- For proton-rich halo nuclei, the long tail manner was clearly seen in the calculated $\rho_p(r)$ and $\rho_m(r)$.

11. References

[1] I. Tanihata, *Prog. Part Nucl. Phys.,* **35**, (1995), 505.

[2] H. Geissel, G. M¨unzenberg and K. Riisager, *Annu. Rev. Nucl. Part. Sci.,* **45**, (1995), 163.

[3] A. Mueller, *Prog. Part. Nucl. Phys.,* **46**, (2001) 359.

[4] Z. Wang, Z. Ren and Y. Fan, *Phys. Rev.,* **C73**, (2006) 014610.

[5] H. Aytekin, E. Tel and R. Baldik, *Turk J Phys* **32** (2008) 181.

[6] A. N. Abdullah, Ph.D. Thesis, University of Baghdad (2015).

[7] T. Moriguchi, Ph. D.Thesis, University of Tsukuba (2011).

[8] I. Talmi and I. Unna, *Phys. Rev. Lett.* **4** (1960) 469; P G Hansen; *Nucl. Phys. A* **682** (2001) 310.

[9] J. Dobaczewski *et al., Phys. Rev. C* **53** (1996) 6.

[10] D. Lee, Ph.D.Thesis, University of California, Berkeley (2007).

[11] T. Leontiou, Ph.D. Thesis, University of Manchester Institute of Science and Technology, UK, (2004).

[12] M. Hemalatha, S. Kailas and Y. K. Gambhir , *Hyperfine Interactions* **162** (2005)133.

[13] I. Tanihata , *Nucl. Phys. A* **654** (1999) 235c.

[14] G.W. Jun *et al., Commun. Theor. Phys.* **40** (2003) 577.

[15] I. *Tanihata et al., Phys. Rev. Lett.* **55** (1985) 2676.

[16] P. G. Hansen and B. Jonson, *Euro. Phys. Lett.* **4** (1987) 409.

[17] M. Labiche *et al. Phys. Rev. Lett.* **86** (2001) 600.

[18] D. Q. Fang *et al., Phys. Rev. C* **69**, 034613 (2004).

[19] K. Tanaka *et al., Phys. Rev. Lett.* **104**, (2010) 062701.

[20] P. Egelhof, *Prog. Part. Nucl. Phys.* **46** (2001) 307.

[21] P. G. Hansen, A. S. Jensen and B. Jonson, *Annu. Rev. Nucl. Part. Sci.* **45** (1995) 591.

[22] I. Tanihata, *Nucl. Phys. A* **520** (1990) 411c.

[23] H. Y. Zhang *et al., Nucl. Phys. A* **707** (2002) 303.

[24] A. Dadi, Ph.D. Thesis, Ruperto-Carola University of Heidelberg, Germany, (2012).

[25] A. Y. A. Alsajjad M. Sc. Thesis, University of Baghdad (2020).

[26] G.W. Jun *et al., Commun. Theor. Phys.* **40** (2003) 577.

[27] H. Z. Guo *et al., Sci. China. Ser. G, Phys. Mech. Astron.* **51** (2008) 781.

[28] J. Al-Khalili, The Euroschool Lectures on Physics with Exotic Beams (I) (2004) 77-112.

[29] D. Borremans, Ph.D. Thesis, Katholieke University (2004).

[30] I. Tanihata *et al., Phys. Lett. B* **160** (1985) 380.

[31] I. Tanihata, T. Kobayashi, O. Yamakawa, et al., Phys. Lett. B 206 (1988) 592.

[32] T. Suzuki, H. Sagawa, K. Hagino, Phys. Rev. C 68 (2003) 014317.

[33] I. Tanihata, H. Savajols and R. Kanungo, *Prog. Part. Nucl. Phys.* **68** (2013) 215.

[34] A.V. Dobrovolsky *et al., Nucl. Phys. A* **766** (2006) 1.

[35] P. Egelhof *et al., Euro. Phys. J. A* **15** (2002) 27.

[36] G.D. Alkhazov *et al., Nucl. Phys. A* **712** (2002) 269–299.

[37] K. Tanaka, et al., Phys. Rev. C **82** (2010) 044309.

[38] A. K. Hamoudi, G. N. Flaiyh, A. N. Abdullah, Iraqi Journal of Physics 12 (24) (2014) 10.

[39] A. K. Hamoudi and A. N. Abdullah, Iraqi Journal of Science 57 (2016) 2664.

[40] H. Du *et al., Acta Physica Polonica* B 48 (3) (2016) 473.

[41] A. N. Abdullah, International Journal of Modern Physics E **26,** 1750048 (2017)

[42] G. A. Korolev *et al.,* Phys. Lett. B 780, 200 (2018).

[43] A. N. Abdullah, Iraqi Journal of Science 59 (2c) (2018) 1057.

[44] A. N. Abdullah, *Int. J. Mod. Phys. E* 29 (2020) 2050015.

[45] A. N. Abdullah, *Mod. Phys. Lett. A* 35 (2020) 2050212.

[46] A. N. Abdullah, *Physics of Atomic Nuclei* 83 (2020) 785.

[47] L. F. Sultan and A. N. Abdullah, Iraqi Journal of Physics, (2021) 21.

[48] G. M. Sallh and A. N. Abdullah *Iraqi Journal of Science,* **62** (8) (2021) 2555.

[49] H. K. Mahdi, A. N. Abdullah *Iraqi Journal of Physics*, **20** (4) (2022) 18.

[50] A. N. Abdullah, *Int. J. Mod. Phys. E* **31** (2022) 2250076.

[51] H. K. Mahdi, A. N. Abdullah, *AIP Conf. Proc.*, **2977** (2023) 040080-1.

[52] H. K. Mahdi, A. N. Abdullah, *AIP Conf. Proc.*, **2977** (2023) 040118-1.